

Article

Impact of the Indo-Pacific Warm Pool on the Hadley, Walker, and Monsoon Circulations

Hye-Ryeom Kim ¹, Kyung-Ja Ha ^{1,2,*}, Suyeon Moon ^{2,3}, Hyeun Oh ⁴ and Sahil Sharma ^{2,3}

¹ Department of Atmospheric Sciences, Pusan National University, Busan 46241, Korea; hyeryeom@pusan.ac.kr

² Center for Climate Physics, Institute for Basic Science (IBS), Busan 46241, Korea; suyeon@pusan.ac.kr (S.M.); sahils@pusan.ac.kr (S.S.)

³ Department of Climate System, Pusan National University, Busan 46241, Korea

⁴ Irreversible Climate Change Research Center, Yonsei University, Seoul 03722, Korea; heunoh@yonsei.ac.kr

* Correspondence: kjha@pusan.ac.kr; Tel.: +82-051-510-7860

Received: 21 August 2020; Accepted: 22 September 2020; Published: 24 September 2020



Abstract: The Indo-Pacific warm pool (IPWP) is enclosed by a 28 °C isotherm and plays a vital role in controlling atmospheric circulations. However, the effects of changes in regional warm pool sea surface temperatures (SSTs) remain unexplored. We divided the IPWP into the Indian and Pacific sectors and distinguished their responses to natural variability and global warming. Furthermore, we examined the impacts of the interannual variability (IAV) in warm pool SST on the tropical Hadley, Walker, and monsoon circulations. The Hadley circulation was affected by warm pool SST warming, i.e., warmer SSTs over the warm pool strengthened the upward branch of Hadley circulation, whereas the downward branch was respectively weakened and strengthened in the Northern and Southern Hemispheres. Walker circulation was strengthened (weakened) in the warming (natural) mode. Consequently, the Walker circulation is weakened since the natural variability of warm pool SST plays a more dominant role rather than the warming trend of SSTs over the warm pool. Furthermore, our analysis displays that warm pool warming has little impact on the monsoon circulation. Our findings highlight the different roles of the IAV of warm pool regions in each tropical circulation as part of the warming trend and natural variability.

Keywords: warm pool intensity; Hadley circulation; Walker circulation; monsoon circulation

1. Introduction

The Indo-Pacific warm pool (IPWP), comprising the eastern tropical Indian and western tropical Pacific Oceans, straddles the equator and adjacent regions. It is the largest expanse of warm water with sea surface temperatures (SSTs) consistently exceeding 28 °C [1–3], which is the threshold temperature for atmospheric deep convection [4,5]. The IPWP plays a key role as a major energy source, supplying heat and water vapor through deep convection, which leads to intense air–sea interactions [6–8]. Thus, this warm pool can elucidate ocean–atmosphere couplings [9,10]. In particular, the IPWP plays two important roles in the global climate. First, since saturation vapor pressure is an exponential function of SST [5,11], the intensity of atmospheric deep convection is influenced by changes in IPWP SST. This may cause global climate anomalies and disasters due to unstable atmospheric conditions [12–14]. Second, SST variations in the IPWP are closely linked to upward motion. Even small variations in IPWP SST can bring about considerable changes in the global climate and may directly affect Hadley and Walker circulations [12,15–17].

The warm pool SST interacts with others (such as El Niño–Southern Oscillation (ENSO) and Pacific Decadal Oscillations (PDO)) and contributes to climate variability at interannual, decadal,

and millennial scales [18–21]. Quinn et al. [22] found that interannual variability (IAV) in the western Pacific warm pool is closely related to ENSO variation based on coral $\delta^{18}\text{O}$ and Sr/Ca time series data. Lin et al. [20] showed that the thermal variations in the IPWP are mostly influenced by the PDO. Long-term thermal and hydrological fluctuations in the IPWP have been spotlighted since the early 2000s. From the last glacial period to the Holocene, an intimate relationship has been observed between the IPWP SST, Asian–Australian monsoon system, and sea level [23–25]. During cold events, the warmer southern part of the IPWP weakens the southern hemispheric limb of the Hadley circulation, decreasing the Asian monsoon rainfall [14]. Although efforts have been made to understand the IAV in each warm pool, the role of IAV in warm pool SST in tropical circulations remains poorly understood.

Most studies have focused on the Pacific warm pool (PWP) [1,25–27], but the Indian warm pool (IWP) is also an important part of IPWP. Several studies have examined the seasonal variations and IAV in warm pool properties and compared the Pacific and Indian Oceans [28,29]. Kim et al. [28] indicated that the PWP and IWP differ in terms of size, mean and maximum SST, and latitudinal and longitudinal centers. On a seasonal timescale, the IWP has a distinctive seasonal cycle in terms of mean and maximum SSTs and size, whereas the IAVs in the IWP and PWP are comparable. Besides, the edge location of the warm pool changes seasonally, but only longitudinal displacements are delicate to IAVs. Furthermore, the seasonal variability in the Pacific Ocean is controlled by the annual orbit of the sun, and the Indian Ocean is affected by the Indian summer monsoon [28,30]. Therefore, research on each warm pool region is urgently needed.

The IPWP is particularly vulnerable to anthropogenic greenhouse forcing [31–33], and IPWP SST is expected to increase [34]. With global warming, warmer warm pool SST can affect atmospheric circulation. According to Feng et al. [17], Hadley circulation is more sensitive to a warmer IPWP than a colder IPWP. Thus, continuous IPWP warming renders the Hadley cell more sensitive to tropical SST [17]. IPWP warming since the 1950s has been proposed to intensify Hadley circulation during boreal winter [35]. Besides, a large ensemble of model simulations has shown that internal variability plays a dominant role in the recent strengthening of the Pacific Walker Circulation (PWC). The Interdecadal Pacific Oscillation (IPO) and Atlantic Ocean warming are suggested to be the main factors affecting changes in the PWC [36]. Therefore, the modulations of each circulation arise from different conditions. In this study, we investigated the impacts of IAVs in the IPWP, IWP, and PWP on tropical circulations, namely Hadley, Walker, and monsoon circulations, via linear trends and detrended parts thereof.

The remainder of this paper is organized as follows. In the next section, we describe the dataset and definitions used in this study. In Section 3, we examine SST trends in each warm pool region and their IAVs. Section 4 presents the relationship between warm pool intensity and tropical circulations with or without a linear trend. Finally, Section 5 discusses and summarizes the results.

2. Data and Methods

We used monthly mean zonal wind at 850 and 200 hPa and omega at 500 hPa, provided by the European Center for Medium-Range Weather Forecasts (ECMWF) Interim reanalysis products [37]. Monthly precipitation was obtained from the Global Precipitation Climatology Project version 2.3 (GPCPv2.3) with a $2.5^\circ \times 2.5^\circ$ horizontal resolution [38]. For SST analysis, the Hadley Centre Sea Ice and Sea Surface Temperature (HadISST) [39] was used. Also, we used interpolated outgoing longwave radiation (OLR) monthly data retrieved from the National Oceanic and Atmospheric Administration (NOAA) satellite series [40]. All datasets were interpolated onto a 2.5° grid through a bilinear interpolation technique for the period from 1979 to 2018.

Figure 1a,b show the warm pool regions where SSTs are above 28°C climatologically. One is the IPWP and the other is the tropical Western Hemisphere warm pool near the Intra-Americas Sea (Figure 1a,b). In this study, we only focused on the IPWP. To investigate regional warm pool SST, the IPWP was divided into Indian and Pacific sectors. According to Weller et al. [41], the IPWP region is delineated by the 28°C isotherm between 25°S – 25°N and 40°E – 130°W . The IWP and PWP were

distinguished by the 120° E meridian (Figure 1a) [41]. The warm pool intensity was defined by the averaged SST anomaly within each warm pool region. A 12-month annual mean was subsequently calculated from June to following May for the successive ENSO effect.

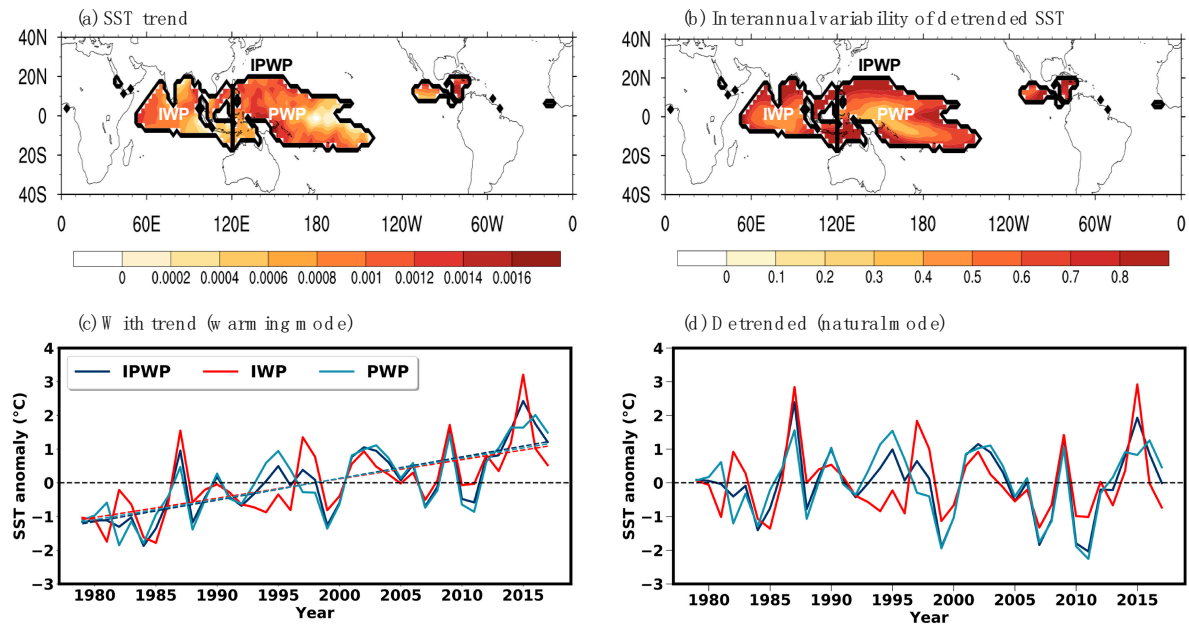


Figure 1. Indo-Pacific warm pool (IPWP) regions delineated by 28 °C isotherm between 25° S–25° N and 40° E–130° W (black solid lines). IPWP was divided into Indian and Pacific sectors by 120° E meridian. (a) The trend of sea surface temperature (SST) from 1979 to 2018 (shading, K/40 years). (b) The interannual variability of detrended SST during the same period (shading). (c) Time series of each normalized warm pool intensity (solid lines) with their respective trends (dashed lines). The 12-month annual mean was implemented for the warm pool intensity. (d) Detrended time series of each normalized warm pool intensity. Blue, red, and sky-blue lines indicate the IPWP, Indian warm pool (IWP), and Pacific warm pool (PWP), respectively.

To identify the features of large-scale tropical circulations, such as the Hadley, Walker, and monsoon circulations, a velocity potential of 200 hPa was used. The velocity potential of the upper troposphere can represent the large-scale characteristics of the tropical circulations and the overall intensity [42]. The centers of regions with positive (negative) velocity potential at 200 hPa denote the upper-level divergence (convergence), respectively. To compare and quantify intensities of three different atmospheric circulations, the intensity of each circulation is defined by their peak values of velocity potential referred to Tanaka et al. [42]. For the sake of simplicity, the unit of the velocity potential was quantified as $10^5 \text{ m}^2 \text{ s}^{-1}$. Based on the space–time domain, the velocity potential in the upper troposphere can be separated into three parts, following linear combinations of three orthogonal spatial patterns which are introduced by Tanaka et al. [42]:

$$\begin{aligned} \chi(t, x, y) &= [\chi(t, y)] + \chi^*(t, x, y), \\ &= [\chi(t, y)] + \bar{\chi}^*(x, y) + \chi^{*'}(t, x, y). \end{aligned} \tag{1}$$

The first line of the equation indicates that the upper-level divergence field is divided into zonal-mean and eddy components. In the second line, the eddy component is decomposed into its time-mean and transient parts. On the right-hand side of the second line, each part was defined as Hadley, Walker, and monsoon circulations, respectively, in this study. Specifically, Hadley circulation is denoted by the zonal-mean field of the velocity potential, i.e., $[\chi(t, y)]$, where $[\]$ is the zonal-mean field. Walker and monsoon circulations should be contained in the deviation from the zonal mean, i.e., $\chi^*(t, x, y)$, where $()^*$ represents the deviation from the zonal mean, and x, y , and t indicate the

longitude, latitude, and time, respectively. The deviation field is divided into Walker and monsoon circulations, defined by the annual mean, i.e., $\overline{(\)}$, and its deviation, i.e., $(\)'$. Monsoon circulation includes seasonal cycles.

3. Global Warming vs. Natural Variability in Indo-Pacific Warm Pool

The IPWP has been warming during the last 40 years. Figure 1a displays the trend of SST over warm pool regions (Figure 1a). Figure 1b shows the spatial distribution of the IAV for detrended SST within the warm pool. For the IAV, the deviation is large in the warm pool boundary region (Figure 1b). Figure 1c,d present the IAV in each warm pool intensity, including the linear trend and detrended data, respectively. Including the linear trend, the correlation coefficients of the IPWP and PWP, and IWP intensity were 0.95 and 0.88, respectively. In detrended cases, the corresponding correlation coefficients were 0.91 and 0.46, respectively (at the 99% confidence level). Regardless of the presence of trends, the IAV in the IPWP intensity was controlled by PWP variability. The IPWP and IWP relationship with detrended data had become weaker than that with the linear trend. In other words, the IAV in the PWP intensity was more dominant than that in the IPWP intensity without a linear trend.

Warm pool intensities in all regions showed warming trends (Figure 1c). This supported previous findings that the IPWP has been warming and expanding, especially in recent decades [27,43–45]. Some studies have shown that greenhouse gases are the main cause of increasing global ocean temperature [46,47]. Roxy et al. [48] reported that continuous warming of the IPWP is attributable to both anthropogenic and natural forcing. Based on observations, the Indian Ocean has shown consistent warming, particularly in recent decades [49–51]. Even though greenhouse gases are a major reason for Indian Ocean warming by triggering changes in air–sea fluxes, the net surface heat fluxes over the IWP area alone cannot account for the continuous warming. Rather, an ocean–atmosphere coupled positive feedback through oceanic Rossby waves, not just the greenhouse warming effect, is responsible for the consistent warming and expansion of the IWP [43]. Each warming trend accounted for 37.94, 26.12, and 31.12% of the total IAVs in the IPWP, IWP, and PWP, respectively. The linear trend comprised a large portion of the total deviation in the IPWP, indicating that the warming effect explained a substantial portion of the IAV in the warm pool SST. In this study, the linear trend of warm pool intensity was regarded as the warming mode, and the detrended part of warm pool intensity was considered the natural mode. The modulation of tropical circulations associated with the IAVs in warm pool SSTs in warming and natural modes is of particular interest

4. Impact of Warm Pool Intensity on Tropical Circulation

4.1. Hadley Circulation

Hadley circulation is thermally driven and plays a significant role in climate systems. As Hadley circulation bridges the tropics and subtropics, changes in its width or intensity exert a substantial influence on the global climate [52,53]. Hadley circulation was assumed by an axisymmetric part of the circulation [42]. Seasonally, the positive peak of the velocity potential at 200 hPa in the Northern Hemisphere occurred at 15° N with 39 units, whereas the negative peak appeared at 25° S with –46 units in boreal summer (not shown). During boreal winter, the center of the sinking motion was located at 25° N, with a peak value of –41 units, and a rising motion occurred at 10° S, with a peak of 37 units (not shown). The positive and negative peaks indicated the locations of the ascending and descending motions, respectively. The annual velocity potential was positive, with a peak value of 12 units at 4° N. Two negative peaks in the velocity potential appeared at 26° S and 26° N, with 14.2 and –5.6 units, respectively (Figure 2). These results were consistent with the ascending limb of Hadley circulation near the thermal equator, combined with two subsidence regions located between latitudes of 20° and 30° in each hemisphere [29].

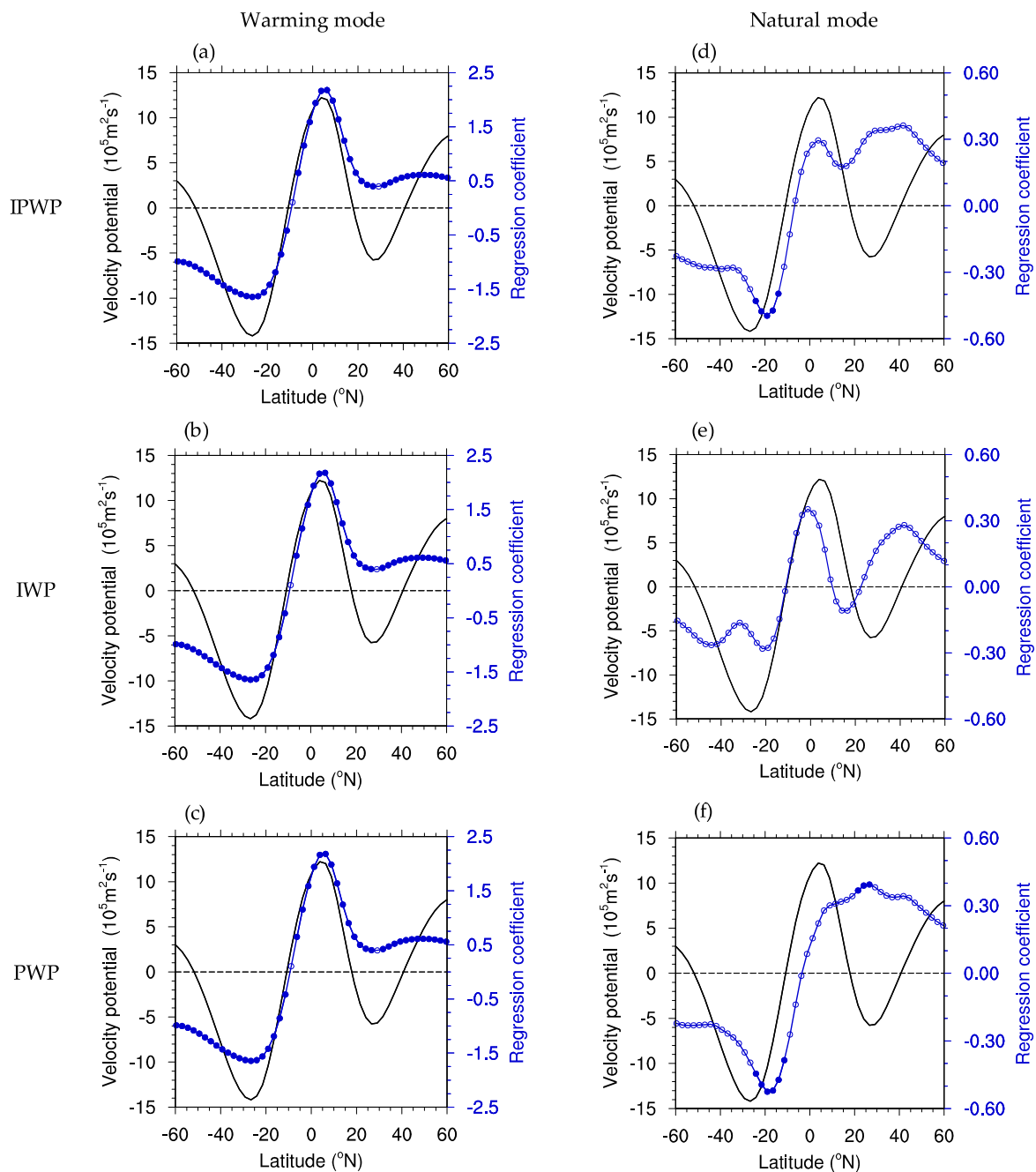


Figure 2. Regression plots of velocity potential anomaly at 200 hPa against the warming trend of warm pool intensity (left column; warming mode) and detrended of each normalized warm pool intensity (right column; natural mode). Three rows indicate that the regression is against (a,d) Indo-Pacific warm pool (IPWP), (b,e) Indian warm pool (IWP), and (c,f) Pacific warm pool (PWP). Negative and positive x -axis values respectively denote Southern and Northern Hemispheres. Black lines denote the annual climatology of the zonal-mean field of 200 hPa velocity potential ($10^5 \text{ m}^2 \text{ s}^{-1}$) in 1979–2018. The blue lines show regression coefficients. Filled blue dots indicate statistical significance at 95% confidence level (Student’s t -test).

Linear regression was used to investigate the effects of IAV in the warm pool intensity on Hadley circulation. In the warming mode, the upward motion tended to be strengthened over the equator, with higher SSTs in the IPWP, IWP, and PWP. When warm pool intensities were strong, the downward motion was respectively weakened or intensified in the Northern or Southern Hemispheres, with a 95% confidence level (Figure 2a–c). In the natural mode, the IWP intensity was not significantly related to

Hadley circulation (Figure 2e). The PWP intensity induced sinking motion in the Southern Hemisphere but diminished descending motion near 20° N in the Northern Hemisphere (Figure 2f).

Likewise, warmer SST in the IPWP strengthened subsidence near 20° S (Figure 2d). Watt-Meyer et al. [54] pointed out differences between the response of Hadley cell expansion in the Northern and Southern Hemispheres under CO₂-induced warming. Accordingly, the Hadley cell in the Southern Hemisphere expanded twice as much as that in the Northern Hemisphere under warming conditions [54]. Greenhouse gas forcing also tends to induce more surface and Arctic mid-tropospheric warming [55]. This might weaken the poleward shift of the eddy-driven jet, which indicates the northern boundary of Hadley circulation in the Northern Hemisphere by decreasing meridional surface temperature gradients [56,57]. On the other hand, warming of the Southern Ocean is delayed at high latitudes, resulting in larger equator-to-pole temperature gradients [58,59] and intensifying the poleward shift of the Hadley circulation edge together with a strong eddy-driven jet in the Southern Hemisphere. This corresponds with different responses of the Hadley cell between the hemispheres, including the warming trend of the warm pool. In addition, several studies suggest that the stratospheric ozone depletion contributes to the Hadley cell expansion in the Southern Hemisphere [60–64]. Based on the coupled model intercomparison projection phase 5 (CMIP5), stratospheric ozone depletion induces significant poleward expansion of the Hadley cell in the Southern Hemisphere [64]. Thus, the asymmetry between the hemispheres might be explained by the mechanisms suggested by Watt-Meyer et al. as well as the stratospheric ozone depletion [54,60–64].

In summary, the SSTs in warm pool regions impact Hadley circulation in the warming mode, but the IWP plays a minor role without the warming trend. Moreover, the Hadley circulation shows a hemisphere asymmetric response to warm pool warming.

4.2. Walker Circulation

Figure 3 shows the regressed patterns of the 12-month annual mean of the zonal deviation velocity potential field at 200 hPa against the warm pool intensities with or without the linear trend. Regarding the 39-year annual climatology (1979–2017), the core of the ascending PWC branch was located over the equatorial western Pacific Ocean with a peak value of approximately 110 units, and the descending branch was located over the equatorial eastern Pacific Ocean with a peak value of –50 units. In the warming mode, the warming trend over the warm pool contributed to the strengthening of the PWC. It induced more upper-level divergence over the western Pacific and more convergence at 200 hPa over Africa and the eastern Pacific Ocean (Figure 3a–c). This concurs well with Kim et al.'s [65] findings that strengthening of PWC is caused by SST warming. Additionally, anomalous upper-level divergence was shown over the northern part of South America in the warming mode. Independent of the warming trend, the strong warm pool intensity of all warm pool regions significantly weakened the upper-level divergence, i.e., the western part of the upper-level divergence core, and strengthened divergence over the eastern part (Figure 3d–f).

Generally, the warming and natural modes showed the opposite regressed patterns and the magnitudes were much stronger for the latter than the former. Considering both the warming trend and natural variability, the results were mostly affected by the natural modes (not shown). Therefore, natural variability had a greater influence on the PWC than the warming effect did. The IPO could be an important factor in modulating the changes in the PWC, because it constitutes major internal variability over the Pacific Ocean [36]. Similarly, the IPO index was calculated based on the difference between the area-averaged SST anomaly over the central equatorial, northwest, and southwest Pacific Ocean [66]. Subsequently, the correlation coefficients between the IPO and natural variability in the warm pool intensities were performed to confirm their relationships. For the detrended case, the correlation coefficients of the IPO and warm pool intensity index were approximately 0.64, while the correlation coefficients were 0.26 including the warming trend. In the African tropical savannah region, however, the warming mode was dominant, and higher SSTs in warm pool regions intensified upper-level convergence (Figure 3a–c).

Similar results were found for the omega anomaly at 500 hPa (Figure 4). In the case of the natural mode, the anomalous rising flow arose over the equatorial central Pacific Ocean. In contrast, the upward motion weakened over the equatorial western Pacific Ocean and Maritime Continent (Figure 4d–f). In the warming mode, anomalous sinking motion was found over the equatorial Africa region (Figure 4a–c). This was consistent with the upper-level convergence shown in Figure 3a–c. To investigate the convective activity, we analyzed the OLR, which yields useful information regarding the convection. A negative or positive OLR value indicates convection or subsidence, respectively. In the tropics, the mean annual OLR cycle is dominated by changes in cloudiness and has a strong negative correlation with precipitation [67]. Figure 5 shows the anomalous OLR associated with the warm pool intensity of the IPWP, IWP, and PWP. When it comes to the natural mode, most cases indicated that positive OLR anomalies significantly were found over the subtropical western Pacific Ocean and Maritime Continent, whereas more convection occurred over the equatorial central Pacific Ocean (Figure 5d–f).

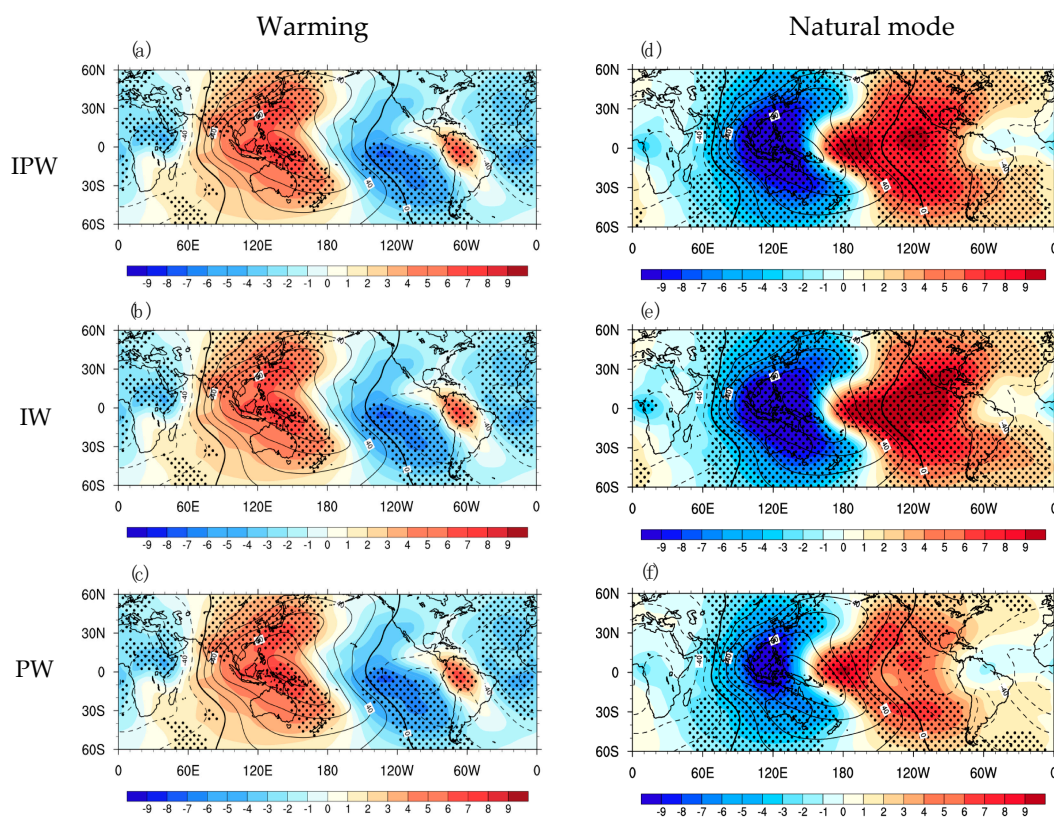


Figure 3. Regressed spatial distribution of velocity potential (shading, $10^5 \text{ m}^2 \text{ s}^{-1}$) anomaly at 200 hPa against the warming trend of warm pool intensity (left column; warming mode) and detrended of each normalized warm pool intensity (right column; natural mode). Three rows indicate that the regression is against (a,d) Indo-Pacific warm pool (IPWP), (b,e) Indian warm pool (IWP), and (c,f) Pacific warm pool (PWP). The black line denotes the climatology of the 12-month annual mean zonal deviation field of 200 hPa velocity potential in 1979–2018. The dotted lines indicate negative velocity potential values, which show upper-level convergence. Black dots indicate statistical significance at 95% confidence levels (Student’s *t*-test).

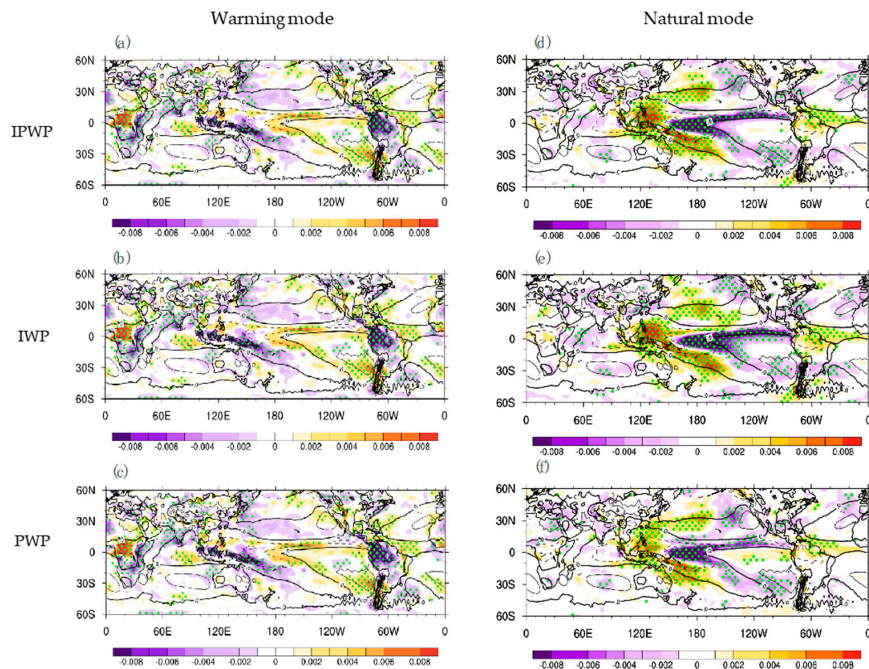


Figure 4. Regressed spatial distribution of 12-month annual mean omega (shading, Pa s^{-1}) anomaly at 500 hPa against the warming trend of warm pool intensity (left column; warming mode) and detrended of each normalized warm pool intensity (right column; natural mode). Three rows indicate that the regression is against (a,d) Indo-Pacific warm pool (IPWP), (b,e) Indian warm pool (IWP), and (c,f) Pacific warm pool (PWP). Black lines denote the climatology of omega at 500 hPa. The dotted lines indicate negative omega values, representing rising motion. Black dots indicate statistical significance at 95% confidence levels (Student’s *t*-test).

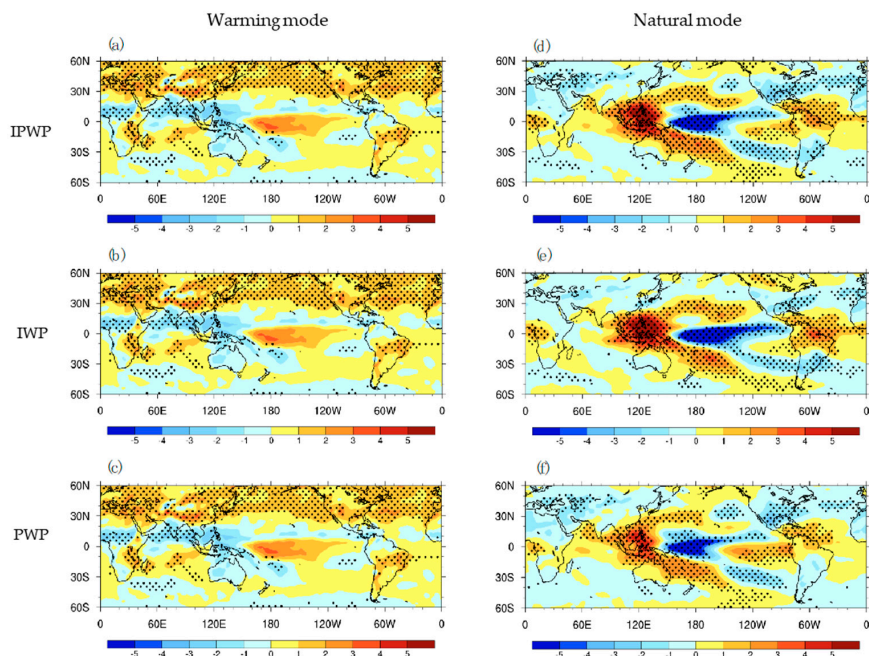


Figure 5. Regressed spatial distribution of 12-month annual mean outgoing longwave radiation (OLR) (shading, W m^{-2}) anomaly against the warming trend of warm pool intensity (left column; warming mode) and detrended of each normalized warm pool intensity (right column; natural mode). Three rows indicate that the regression is against (a,d) Indo-Pacific warm pool (IPWP), (b,e) Indian warm pool (IWP), and (c,f) Pacific warm pool (PWP). Black dots indicate statistical significance at 95% confidence levels (Student’s *t*-test).

Likewise, anomalous precipitation patterns matched OLR patterns over the tropics (Figure 6). The anomalous increasing or decreasing precipitation was consistent with anomalous ascending or descending motion, respectively, in the 500 hPa omega anomaly, 200 hPa velocity potential, and OLR anomaly. In the warming mode, precipitation tended to increase over the tropical western Pacific (Figure 6a–c). Without the warming trend, anomalous decreasing precipitation occurred over the tropical western Pacific, while anomalous increasing precipitation was shown over the central Pacific (Figure 6d–f). As one of the indicators of strengthening (weakening) Walker circulation, anomalous easterlies (westerlies) at 850 hPa can be used [68]. For the warming mode, the anomalous easterly wind was presented over the equatorial Pacific, which means the intensification of the PWC. In contrast, the anomalous westerly wind was shown from the western to central Pacific, indicating the slowdown of the PWC.

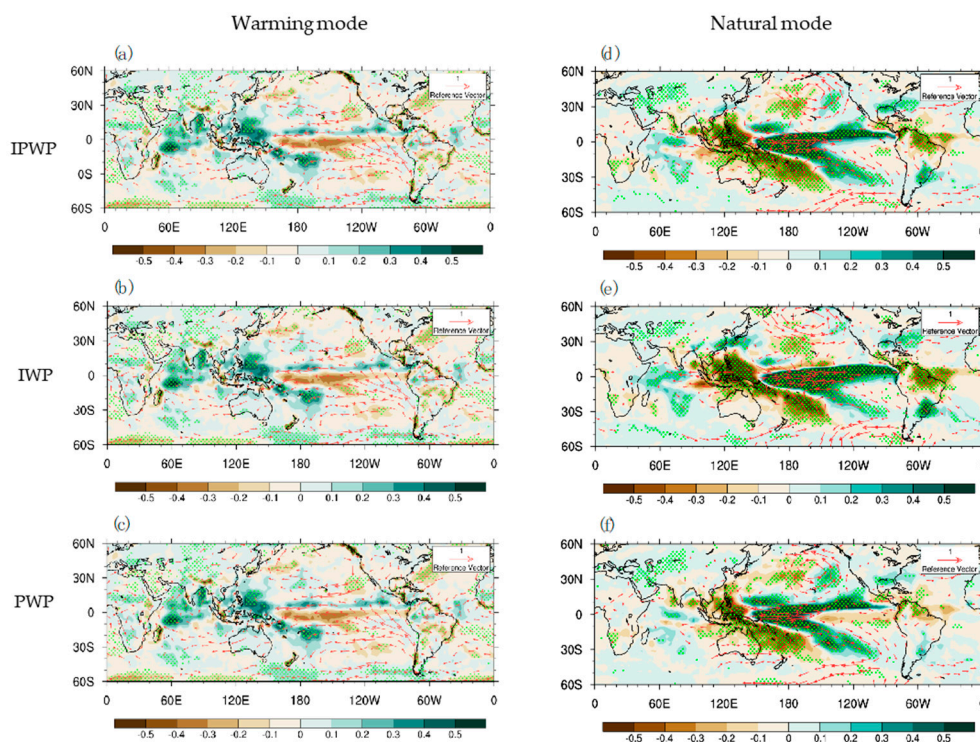


Figure 6. Regressed spatial distribution of 12-month annual mean precipitation (shading, mm day^{-1}) and 850 hPa horizontal wind (vector, m s^{-1}) anomaly against the warming trend of warm pool intensity (left column; warming mode) and detrended of each normalized warm pool intensity (right column; natural mode). Three rows indicate that the regression is against (a,d) Indo-Pacific warm pool (IPWP), (b,e) Indian warm pool (IWP), and (c,f) Pacific warm pool (PWP). Green dots and wind vectors indicate statistical significance at 95% confidence levels (Student's *t*-test).

In conclusion, from the various reanalysis data, changes in the Walker circulation were different in the warming and natural mode. Given the warming trend of SST over the warm pool, the strengthening of the Walker circulation is shown. However, the weakening of the Walker circulation is observed without the linear trend of warm pool intensity. Even though warming and natural mode have different impacts on the Walker circulation, the natural variability plays a dominant role in the modulation of the PWC, whereas Africa is susceptible to the warming trend.

4.3. Monsoon Circulation

Monsoon circulation is regarded as a transient component of zonal deviation fields, which has seasonality. This definition only considers the kinematical circulation of the divergent flow in contrast to the fact that the monsoon in many previous studies is defined by precipitation as thermodynamic

factors [69,70]. Note that the kinematical monsoon circulation is different from the monsoon defined by precipitation which is a function of the moisture and the wind convergence. The kinematically defined monsoon circulation can represent the characteristics of the boreal summer monsoon but does not represent the entity of the monsoon system. Thus, we also see other variables such as omega, OLR, horizontal wind at the lower level, and precipitation. To investigate the impact of the warm pool intensity on the following summer monsoon circulation, the warming trend and detrended of warm pool intensity were regressed onto the following boreal summer (June–August) 200 hPa velocity potential, 500 hPa omega, OLR, and 850 hPa wind and precipitation anomaly.

During boreal summer, a positive peak occurred over the Asian monsoon domain, with a peak value of 82 units (Figure 7). It indicates a strong upward flow with an upper-level divergence concerning the Asian summer monsoon. Compared to JJA climatology, the anomalous dipole pattern of velocity potential at 200 hPa is shown in the Eastern Hemisphere. Under the warming mode, the warming trend of the warm pool does not have conspicuous effects on the boreal summer monsoon circulation (Figure 7a–c). In the natural mode, however, strong IPWP and IWP intensities led to positive anomalies in the upper-level velocity potential over the tropical western Indian Ocean, whereas the negative velocity potential anomalies occurred over the northwestern Pacific Ocean (Figure 7d,e). Higher SST in the PWP diverged over the tropical Indian Ocean significantly, but lower divergence over the northwestern Pacific Ocean was not significant (Figure 7f). In addition, strong IWP intensity led to the weakening of the upper-level divergence in the Western North Pacific monsoon (WNP) region and anomalous upper-level divergence in the North African monsoon (NAF) region under the natural mode (Figure 7e).

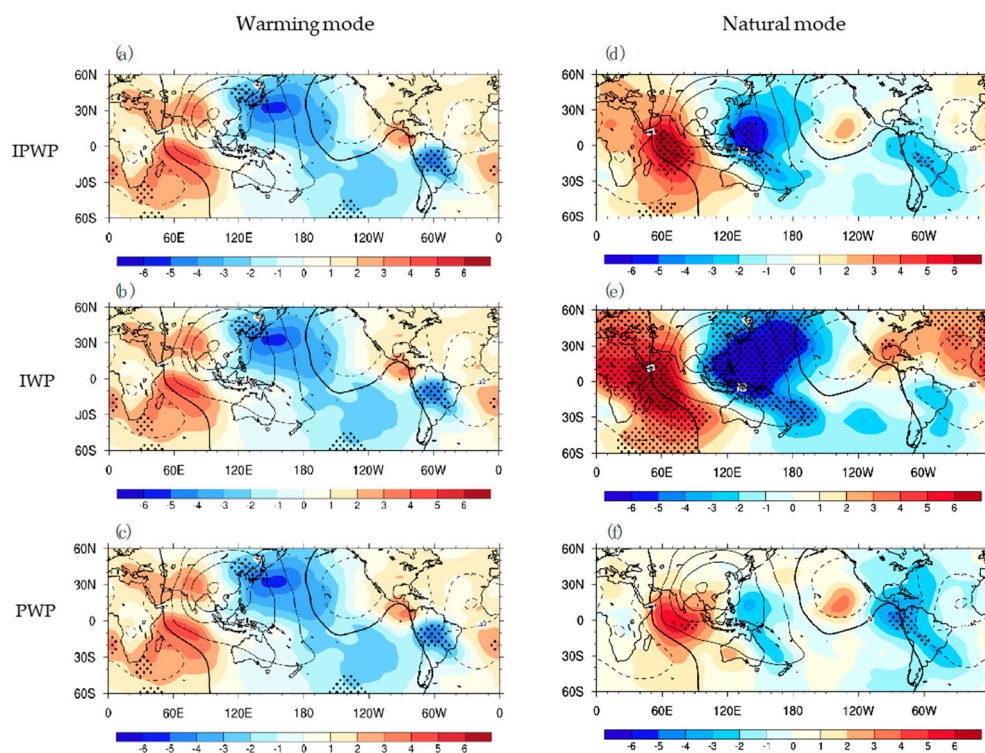


Figure 7. Regressed spatial distribution of June–August (JJA) mean velocity potential (shading, $10^5 \text{ m}^2 \text{ s}^{-1}$) anomaly at 200 hPa, for boreal monsoon circulation, against the warming trend of warm pool intensity (left column; warming mode) and detrended of each normalized warm pool intensity (right column; natural mode). Three rows indicate that the regression is against (a,d) Indo-Pacific warm pool (IPWP), (b,e) Indian warm pool (IWP), and (c,f) Pacific warm pool (PWP). Black lines denote JJA climatology of 12-month annual mean zonal deviation field at 200 hPa velocity potential for 1980–2017. The dotted lines show negative values of velocity potential, indicating upper-level convergence. Black dots indicate statistical significance at 95% confidence levels (Student’s *t*-test).

In terms of vertical motion associated with warm pool intensity, greater ascending motion occurred over India under warming conditions (Figure 8a–c). In the natural mode, higher SSTs over warm pool weakened the upward motion over the western Pacific (Figure 8d–f) and warm SSTs over the IWP induced more rising motion over the maritime continent (Figure 8e). The regression pattern of OLR anomaly showed anomalously more active convection over the NAF region with the warming trend (Figure 9a–c), but no significant pattern was found without the warming trend (Figure 9d–f). Moreover, the western Pacific Ocean tended to be weakened convection in the natural mode (Figure 9d–f). Given precipitation and 850 hPa horizontal wind anomaly, anomalous increasing precipitation is consistent with anomalously more convection over the NAF region (Figure 10a–c), while anomalous decreasing precipitation occurred over the western Pacific (Figure 10d–f). Moreover, significant positive precipitation anomalies occurred over India under the warming conditions (Figure 10a–c). It was attributable to an intensified low-level jet over the Arabian sea, which was important in transporting large quantities of moisture to India (Figure 10a–c). According to Kitoh et al. [71], Indian summer monsoon rainfall remarkably increases, while the kinematical circulation decreases under warming condition. Even though the kinematical circulation weakens, precipitation increases because warmer air can contain more moisture. Our results are in good agreement with Kitoh et al.'s [71] findings that changes in the monsoon, which are defined by kinematical circulation and precipitation, can be different under warming.

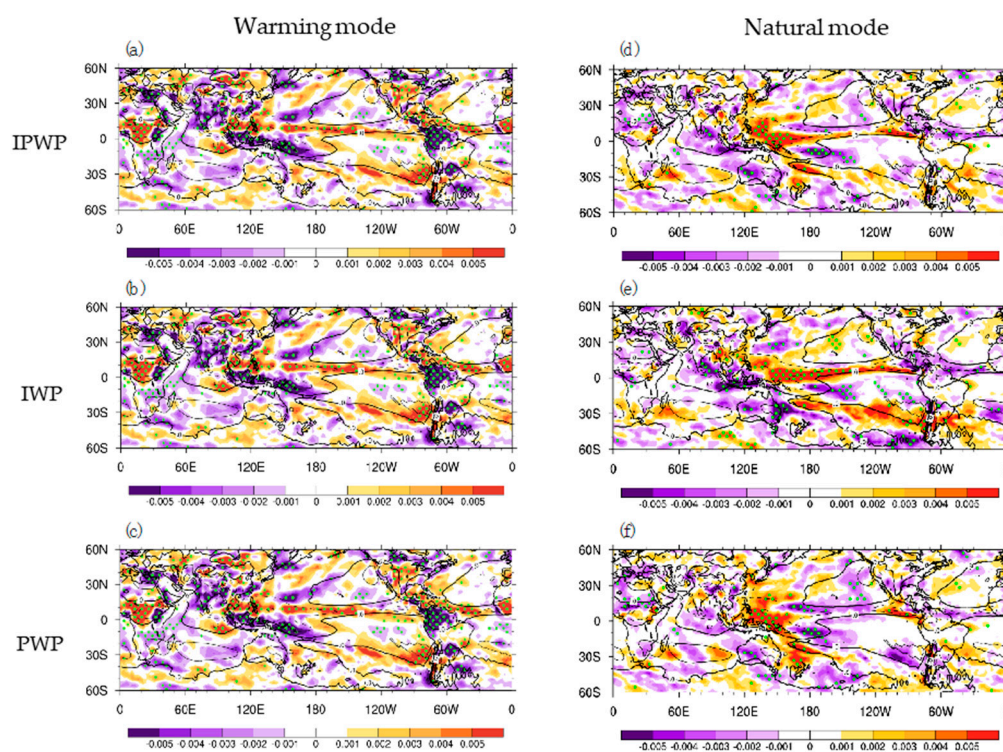


Figure 8. Regressed spatial distribution of June–August (JJA) mean omega (shading, Pa s^{-1}) anomaly at 500 hPa against the warming trend of warm pool intensity (left column; warming mode) and detrended of each normalized warm pool intensity (right column; natural mode). Three rows indicate that the regression is against (a,d) Indo-Pacific warm pool (IPWP), (b,e) Indian warm pool (IWP), and (c,f) Pacific warm pool (PWP). Black lines denote JJA climatology of 500 hPa omega. The dotted lines show negative omega values, indicating rising motion. Black dots indicate statistical significance at 95% confidence levels (Student's *t*-test).

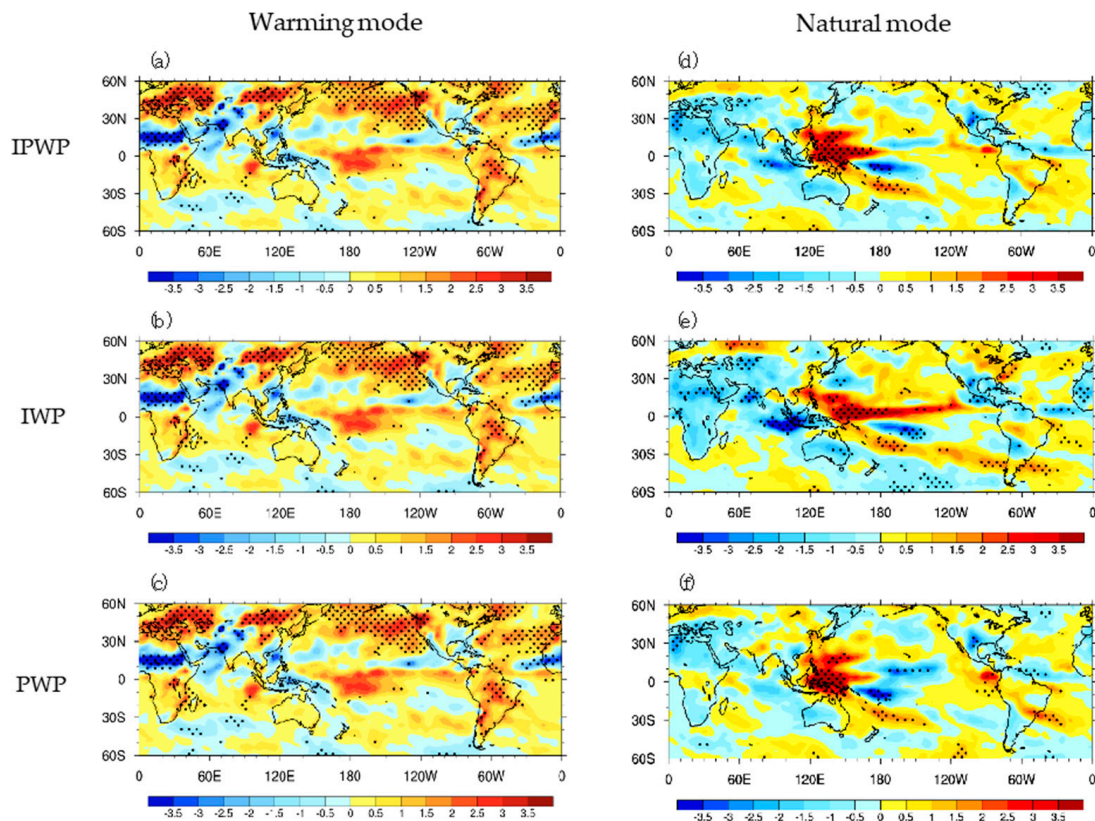


Figure 9. Regressed spatial distribution of June–August (JJA) mean outgoing longwave radiation (OLR) (shading, W m^{-2}) anomaly against the warming trend of warm pool intensity (left column; warming mode) and detrended of each normalized warm pool intensity (right column; natural mode). Three rows indicate that the regression is against (a,d) Indo-Pacific warm pool (IPWP), (b,e) Indian warm pool (IWP), and (c,f) Pacific warm pool (PWP). Black dots indicate statistical significance at 95% confidence levels (Student's *t*-test).

In conclusion, the warming trend of SST over the warm pool did not have a significant role in the modulation of the kinematical monsoon circulation in the boreal summer. In the natural mode, warm pool intensities led to anomalous dipole patterns in the Eastern Hemisphere at the upper-level divergence field. Warmer SST over IWP resulted in the weakening of the upper-level divergence in the WNP region and anomalously increasing upper-level divergence in the NAF region under the natural mode.

To complement the shortcomings of kinematical monsoon circulation, we investigated the impact of warm pool intensity on the precipitation. Warm pool warming strengthened ISM rainfall via a strong low-level jet over the Arabian sea supplying more moisture to India. Furthermore, the warming trend contributed to increasing anomalously more convection and precipitation in the NAF region.

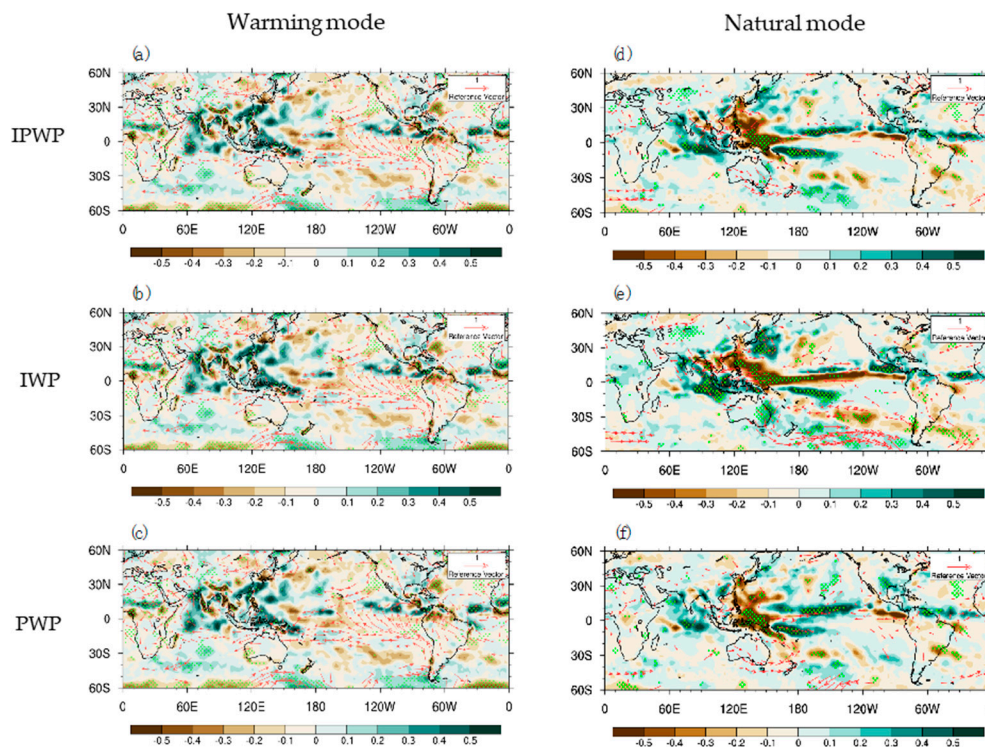


Figure 10. Regressed spatial distribution of June–August (JJA) mean precipitation (shading, mm day^{-1}) and 850 hPa horizontal wind (vector, m s^{-1}) anomaly against the warming trend of warm pool intensity (left column; warming mode) and detrended of each normalized warm pool intensity (right column; natural mode). Three rows indicate that the regression is against (a,d) Indo-Pacific warm pool (IPWP), (b,e) Indian warm pool (IWP), and (c,f) Pacific warm pool (PWP). Green dots and wind vectors indicate statistical significance at 95% confidence levels (Student's *t*-test).

5. Conclusions and Discussion

This study demonstrated that the modulation of tropical circulations was associated with IAVs in warm pool intensity in warming and natural modes. All warm pool regions have been warming in recent decades. The IAV in IPWP intensity could mostly be explained by the IAV in the PWP intensity in both the warming and natural modes. By analyzing atmosphere and ocean reanalysis data, we found that circulations responded differently to warm pool SST in the warming and natural modes. When warm pool SSTs were high, the upward branch of Hadley circulation was strengthened near the equator, and the downward branch respectively weakened or strengthened in the Northern or Southern Hemispheres. Without a linear trend, the IWP intensity did not significantly affect Hadley circulation. That is, the warm pool warming trend was considered the dominant mode of change in Hadley circulation. For Walker circulation, the warming trend of the warm pool tended to strengthen the PWC, while the slowdown of the PWC was found in the natural mode. Considering both the warming and natural effect, the natural variability played a more important role in modulating PWC than the warming effect did. However, Africa was affected more by the warming mode. Under the warming mode, the upper-level convergence was strengthened over equatorial Africa with enhanced descending motion. Regarding boreal summer monsoon circulation, we investigated the role of warm pool intensity in view of both the kinematical circulation and precipitation as representative of the thermodynamic factors. In the warming mode, warm pool warming has a small impact on the kinematical monsoon circulation. For the natural mode, higher SST over IWP affected the WNP region by reducing the upper-level divergence. Additionally, warmer SST over IWP caused anomalous upper-level divergence over the NAF region. In terms of precipitation, the ISM rainfall tended to be enhanced more in the warming mode than the natural mode. This likely resulted from the intensification of the low-level jet

in the western domain of the Arabian Sea, which supplies a great amount of moisture to India during the monsoon period. Moreover, anomalously increasing precipitation was found over the NAF region with warm pool warming.

Since the circulations interacted nonlinearly, there are some limitations to isolating the tropical circulations unambiguously. For the monsoon circulation, there is a discrepancy between the monsoon defined by the kinematical circulation and precipitation. Thus, the results need to be interpreted with caution. Nonetheless, this kinematical separation of the tropical circulations is a useful tool for easily quantifying the intensity of each circulation and investigating the impact of warm pool SST on each tropical circulation.

As a part of key ENSO regions, some investigators presented that changes in the IPWP have a close relationship with the ENSO, which is the most potent source of interannual climate variability [72,73]. According to Wang et al. [73], warming in the IPWP can increase strong El Niño events by strengthening trade winds across the equatorial tropical Pacific. It suggests continuous warming in the IPWP will lead to more frequent extreme El Niño events in the future. In this context, further studies are planned to identify how the variations of the IPWP will affect the tropical circulations in the future. Besides, the considerable influence of warm pool intensity on the regional impact of changes in Hadley circulation necessitates future studies to comprehend the mechanism more appropriately.

The warm pool and its different regions were considered the main components that modulate tropical circulations. Thus, understanding IAVs in the warm pool is essential for understanding the global climate. Our research could benefit investigations on the impact of warm pool intensity on tropical circulations.

Author Contributions: K.-J.H. designed the study and H.-R.K. performed the analysis. All authors contributed to writing the manuscript. All authors have read and agreed to the published version of the manuscript.

Funding: This work was supported by a two-year research grant from Pusan National University.

Acknowledgments: ERA-Interim data can be found at <https://apps.ecmwf.int/datasets/data/interim-full-mnth/levtype=sfc/>; Global Precipitation Climatology Project data at <https://psl.noaa.gov/data/gridded/data.gpcp.html>; NOAA OLR data at https://psl.noaa.gov/data/gridded/data.interp_OLR.html; and HadISST data at <https://climatedataguide.ucar.edu/climate-data/sst-data-hadisst-v11>.

Conflicts of Interest: The authors declare no conflict of interest.

References

1. Yan, X.H.; Ho, C.R.; Zheng, Q.; Klemas, V. Temperature and size variabilities of the Western Pacific Warm Pool. *Science* **1992**, *258*, 1643–1645. [[CrossRef](#)]
2. Chung-Ru Ho; Xiao-Hai Yan; Quanan Zheng Satellite observations of upper-layer variabilities in the western Pacific warm pool. *Bull.-Am. Meteorol. Soc.* **1995**, *76*, 669–680. [[CrossRef](#)]
3. Fasullo, J.; Webster, P.J. Warm pool SST variability in relation to the surface energy balance. *J. Clim.* **1999**, *12*, 1292–1305. [[CrossRef](#)]
4. Zhang, C. Large-Scale Variability of Atmospheric Deep Convection in Relation to Sea Surface Temperature in the Tropics. *J. Clim.* **1993**, *6*, 1898–1913. [[CrossRef](#)]
5. Fu, R.; Del Genio, A.D.; Rossow, W.B. Influence of Ocean Surface Conditions on Atmospheric Vertical Thermodynamic Structure and Deep Convection. *J. Clim.* **1994**, *7*, 1092–1108. [[CrossRef](#)]
6. Visser, K.; Thunell, R.; Stott, L. Magnitude and timing of temperature change in the Indo-Pacific warm pool during deglaciation. *Nature* **2003**, *421*, 152–155. [[CrossRef](#)] [[PubMed](#)]
7. Xie, S.P.; Xu, H.; Kessler, W.S.; Nonaka, M. Air-sea interaction over the eastern Pacific warm pool: Gaps winds, thermocline dome, and atmospheric convection. *J. Clim.* **2005**, *18*, 5–20. [[CrossRef](#)]
8. Duan, A.; Sui, C.; Wu, G. Simulation of local air-sea interaction in the great warm pool and its influence on Asian monsoon. *J. Geophys. Res.* **2008**, *113*. [[CrossRef](#)]
9. Horel, J.D.; Wallace, J.M. Planetary-Scale Atmospheric Phenomena Associated with the Southern Oscillation. *Mon. Weather Rev.* **1981**, *109*, 813–829. [[CrossRef](#)]

10. Webster, P.J. THE ROLE OF HYDROLOGICAL PROCESSES IN OCEAN-ATMOSPHERE Program in Atmospheric and Oceanic Sciences. *Rev. Geophys.* **1994**, *427–476*. [[CrossRef](#)]
11. Graham, N.E.; Barnett, T.P. Sea Surface Temperature, Surface Wind Divergence, and Convection over Tropical Oceans. *Science* **1987**, *238*, 657–659. [[CrossRef](#)]
12. Williams, A.P.; Funk, C. A westward extension of the warm pool leads to a westward extension of the Walker circulation, drying eastern Africa. *Clim. Dyn.* **2011**, *37*, 2417–2435. [[CrossRef](#)]
13. Luo, J.J.; Sasaki, W.; Masumoto, Y. Indian Ocean warming modulates Pacific climate change. *Proc. Natl. Acad. Sci. USA* **2012**, *109*, 18701–18706. [[CrossRef](#)] [[PubMed](#)]
14. Lo, L.; Shen, C.C.; Wei, K.Y.; Burr, G.S.; Mii, H.S.; Chen, M.T.; Lee, S.Y.; Tsai, M.C. Millennial meridional dynamics of the Indo-Pacific Warm Pool during the last termination. *Clim. Past* **2014**, *10*, 2253–2261. [[CrossRef](#)]
15. Prashant, D.; Sardeshmukh, B.J.H. The Generation of Global Rotational Flow by Steady Idealized Tropical Divergence. *J. Atmos. Sci.* **1988**, *45*, 1228–1251.
16. Webster, P.J.; Lukas, R. TOGA COARE: The Coupled Ocean–Atmosphere Response Experiment. *Bull. Am. Meteorol. Soc.* **1992**, *73*, 1377–1416. [[CrossRef](#)]
17. Feng, J.; Li, J.; Kucharski, F.; Wang, Y.; Sun, C.; Xie, F.; Yang, Y. Modulation of the meridional structures of the Indo-Pacific Warm pool on the response of the Hadley Circulation to Tropical SST. *J. Clim.* **2018**, *31*, 8971–8984. [[CrossRef](#)]
18. Cane, M.A. A role for the tropical Pacific. *Science* **1998**, *282*, 59–61. [[CrossRef](#)]
19. Sun, D.-Z.; Fasullo, J.; Zhang, T.; Roubicek, A. On the Radiative and Dynamical Feedbacks over the Equatorial Pacific Cold Tongue. *J. Clim.* **2003**, *16*, 2425–2432. [[CrossRef](#)]
20. Lin, C.-Y.; Ho, C.-R.; Lee, Y.-H.; Kuo, N.-J.; Liang, S.-J. Thermal variability of the Indo-Pacific warm pool. *Glob. Planet. Change* **2013**, *100*, 234–244. [[CrossRef](#)]
21. Ha, K.-J.; Chu, J.-E.; Lee, J.-Y.; Yun, K.-S. Interbasin coupling between the tropical Indian and Pacific Ocean on interannual timescale: Observation and CMIP5 reproduction. *Clim. Dyn.* **2017**, *48*, 459–475. [[CrossRef](#)]
22. Quinn, T.M.; Taylor, F.W.; Crowley, T.J. Coral-based climate variability in the Western Pacific Warm Pool since 1867. *J. Geophys. Res. Ocean.* **2006**, *111*, 1–11. [[CrossRef](#)]
23. Stott, L.; Cannariato, K.; Thunell, R.; Haug, G.H.; Koutavas, A.; Lund, S. Decline of surface temperature and salinity in the western tropical Pacific Ocean in the Holocene epoch. *Nature* **2004**, *431*, 56–59. [[CrossRef](#)]
24. Oppo, D.W.; Rosenthal, Y.; Linsley, B.K. 2000-year-long temperature and hydrology reconstructions from the Indo-Pacific warm pool. *Nature* **2009**, *460*, 1113–1116. [[CrossRef](#)] [[PubMed](#)]
25. Linsley, B.K.; Rosenthal, Y.; Oppo, D.W. Holocene evolution of the Indonesian throughflow and the western Pacific warm pool. *Nat. Geosci.* **2010**, *3*, 578–583. [[CrossRef](#)]
26. Picaut, J.; Ioualalen, M.; Menkes, C.; Delcroix, T.; McPhaden, M.J. Mechanism of the Zonal Displacements of the Pacific Warm Pool: Implications for ENSO. *Science* **1996**, *274*, 1486. [[CrossRef](#)]
27. Cravatte, S.; Delcroix, T.; Zhang, D.; McPhaden, M.; Leloup, J. Observed freshening and warming of the western Pacific Warm Pool. *Clim. Dyn.* **2009**, *33*, 565–589. [[CrossRef](#)]
28. Kim, S.T.; Yu, J.Y.; Lu, M.M. The distinct behaviors of Pacific and Indian Ocean warm pool properties on seasonal and interannual time scales. *J. Geophys. Res. Atmos.* **2012**, *117*, 1–12. [[CrossRef](#)]
29. Yin, Z.; Dong, Q.; Kong, F.; Cao, D.; Long, S. Seasonal and interannual variability of the Indo-Pacific Warm Pool and its associated climate factors based on remote sensing. *Remote Sens.* **2020**, *12*, 1062. [[CrossRef](#)]
30. Kim, S.; Ha, K.J.; Ding, R.; Li, J. Re-examination of the decadal change in the relationship between the East Asian Summer Monsoon and Indian Ocean SST. *Atmosphere* **2018**, *9*, 395. [[CrossRef](#)]
31. Knutson, T.R.; Delworth, T.L.; Dixon, K.W.; Held, I.M.; Lu, J.; Ramaswamy, V.; Schwarzkopf, M.D.; Stenchikov, G.; Stouffer, R.J. Assessment of Twentieth-Century Regional Surface Temperature Trends Using the GFDL CM2 Coupled Models. *J. Clim.* **2006**, *19*, 1624–1651. [[CrossRef](#)]
32. Deser, C.; Phillips, A.S.; Tomas, R.A.; Okumura, Y.M.; Alexander, M.A.; Capotondi, A.; Scott, J.D.; Kwon, Y.-O.; Ohba, M. ENSO and Pacific Decadal Variability in the Community Climate System Model Version 4. *J. Clim.* **2012**, *25*, 2622–2651. [[CrossRef](#)]
33. Zhang, L.; Han, W.; Sienz, F. Unraveling Causes for the Changing Behavior of the Tropical Indian Ocean in the Past Few Decades. *J. Clim.* **2018**, *31*, 2377–2388. [[CrossRef](#)]
34. De Deckker, P. The Indo-Pacific Warm Pool: Critical to world oceanography and world climate. *Geosci. Lett.* **2016**, *3*, 20. [[CrossRef](#)]

35. Quan, X.-W.; Diaz, H.F.; Hoerling, M.P. *Change in the Tropical Hadley Cell Since 1950*; Springer: Dordrecht, The Netherlands, 2004; ISBN 978-1-4020-2944-8.
36. Chung, E.S.; Timmermann, A.; Soden, B.J.; Ha, K.J.; Shi, L.; John, V.O. Reconciling opposing Walker circulation trends in observations and model projections. *Nat. Clim. Chang.* **2019**, *9*, 405–412. [[CrossRef](#)]
37. Dee, D.P.; Uppala, S.M.; Simmons, A.J.; Berrisford, P.; Poli, P.; Kobayashi, S.; Andrae, U.; Balmaseda, M.A.; Balsamo, G.; Bauer, P.; et al. The ERA-Interim reanalysis: Configuration and performance of the data assimilation system. *Q. J. R. Meteorol. Soc.* **2011**, *137*, 553–597. [[CrossRef](#)]
38. Adler, R.F.; Huffman, G.J.; Chang, A.; Ferraro, R.; Xie, P.P.; Janowiak, J.; Rudolf, B.; Schneider, U.; Curtis, S.; Bolvin, D.; et al. The version-2 global precipitation climatology project (GPCP) monthly precipitation analysis (1979–present). *J. Hydrometeorol.* **2003**, *4*, 1147–1167. [[CrossRef](#)]
39. Rayner, N.A.; Parker, D.E.; Horton, E.B.; Folland, C.K.; Alexander, L.V.; Rowell, D.P.; Kent, E.C.; Kaplan, A. Global analyses of sea surface temperature, sea ice, and night marine air temperature since the late nineteenth century. *J. Geophys. Res. Atmos.* **2003**, *108*. [[CrossRef](#)]
40. Liebmann, B.; Smith, C.A. Description of a Complete (Interpolated) Outgoing Longwave Radiation Dataset. *Bull. Am. Meteorol. Soc.* **1996**, *77*, 1275–1277.
41. Weller, E.; Min, S.K.; Cai, W.; Zwiers, F.W.; Kim, Y.H.; Lee, D. Human-caused Indo-Pacific warm pool expansion. *Sci. Adv.* **2016**, *2*, 1–8. [[CrossRef](#)]
42. Tanaka, H.L.; Ishizaki, N.; Kitoh, A. Trend and interannual variability of Walker, monsoon and Hadley circulations defined by velocity potential in the upper troposphere. *Tellus A Dyn. Meteorol. Oceanogr.* **2004**, *56*, 250–269. [[CrossRef](#)]
43. Rao, S.A.; Dhakate, A.R.; Saha, S.K.; Mahapatra, S.; Chaudhari, H.S.; Pokhrel, S.; Sahu, S.K. Why is Indian Ocean warming consistently? *Clim. Change* **2012**, *110*, 709–719. [[CrossRef](#)]
44. Dong, L.; Zhou, T.; Wu, B. Indian Ocean warming during 1958–2004 simulated by a climate system model and its mechanism. *Clim. Dyn.* **2014**, *42*, 203–217. [[CrossRef](#)]
45. Kidwell, A.; Han, L.; Jo, Y.-H.; Yan, X.-H. Decadal Western Pacific Warm Pool Variability: A Centroid and Heat Content Study. *Sci. Rep.* **2017**, *7*, 13141. [[CrossRef](#)] [[PubMed](#)]
46. Gleckler, P.J.; Santer, B.D.; Domingues, C.M.; Pierce, D.W.; Barnett, T.P.; Church, J.A.; Taylor, K.E.; Achutarao, K.M.; Boyer, T.P.; Ishii, M.; et al. Human-induced global ocean warming on a multidecadal timescales. *Nat. Clim. Chang.* **2012**, *2*, 524–529. [[CrossRef](#)]
47. Wijffels, S.; Roemmich, D.; Monselesan, D.; Church, J.; Gilson, J. Ocean temperatures chronicle the ongoing warming of Earth. *Nat. Clim. Chang.* **2016**, *6*, 116–118. [[CrossRef](#)]
48. Roxy, M.K.; Ritika, K.; Terray, P.; Masson, S. The Curious Case of Indian Ocean Warming. *J. Clim.* **2014**, *27*, 8501–8509. [[CrossRef](#)]
49. Lau, K.-M.; Weng, H. Interannual, Decadal–Interdecadal, and Global Warming Signals in Sea Surface Temperature during 1955–1997. *J. Clim.* **1999**, *12*, 1257–1267. [[CrossRef](#)]
50. Hoerling, M.P.; Hurrell, J.W.; Xu, T.; Bates, G.T.; Phillips, A.S. Twentieth century North Atlantic climate change. Part II: Understanding the effect of Indian Ocean warming. *Clim. Dyn.* **2004**, *23*, 391–405. [[CrossRef](#)]
51. Du, Y.; Xie, S.P. Role of atmospheric adjustments in the tropical Indian Ocean warming during the 20th century in climate models. *Geophys. Res. Lett.* **2008**, *35*, 2–6. [[CrossRef](#)]
52. Lindzen, R.S. Climate Dynamics and Global Change. *Annu. Rev. Fluid Mech.* **1994**, *26*, 353–378. [[CrossRef](#)]
53. Chang, E.K.M. The Influence of Hadley Circulation Intensity Changes on Extratropical Climate in an Idealized Model. *J. Atmos. Sci.* **1995**, *52*, 2006–2024. [[CrossRef](#)]
54. Watt-Meyer, O.; Frierson, D.M.W.; Fu, Q. Hemispheric Asymmetry of Tropical Expansion Under CO₂ Forcing. *Geophys. Res. Lett.* **2019**, *46*, 9231–9240. [[CrossRef](#)]
55. Manabe, S.; Stouffer, R.J. Sensitivity of a global climate model to an increase of CO₂ concentration in the atmosphere. *J. Geophys. Res.* **1980**, *85*, 5529–5554. [[CrossRef](#)]
56. Butler, A.H.; Thompson, D.W.J.; Heikes, R. The Steady-State Atmospheric Circulation Response to Climate Change–like Thermal Forcings in a Simple General Circulation Model. *J. Clim.* **2010**, *23*, 3474–3496. [[CrossRef](#)]
57. Barnes, E.A.; Screen, J.A. The impact of Arctic warming on the midlatitude jet-stream: Can it? Has it? Will it? *Wiley Interdiscip. Rev. Clim. Chang.* **2015**, *6*, 277–286. [[CrossRef](#)]
58. Marshall, J.; Armour, K.C.; Scott, J.R.; Kostov, Y.; Hausmann, U.; Ferreira, D.; Shepherd, T.G.; Bitz, C.M. The ocean’s role in polar climate change: Asymmetric Arctic and Antarctic responses to greenhouse gas and ozone forcing. *Philos. Trans. R. Soc. A Math. Phys. Eng. Sci.* **2014**, *372*. [[CrossRef](#)]

59. Armour, K.C.; Marshall, J.; Scott, J.R.; Donohoe, A.; Newsom, E.R. Southern Ocean warming delayed by circumpolar upwelling and equatorward transport. *Nat. Geosci.* **2016**, *9*, 549–554. [[CrossRef](#)]
60. Polvani, L.M.; Waugh, D.W.; Correa, G.J.P.; Son, S.W. Stratospheric ozone depletion: The main driver of twentieth-century atmospheric circulation changes in the Southern Hemisphere. *J. Clim.* **2011**, *24*, 795–812. [[CrossRef](#)]
61. McLandress, C.; Shepherd, T.G.; Scinocca, J.F.; Plummer, D.A.; Sigmond, M.; Jonsson, A.I.; Reader, M.C. Separating the dynamical effects of climate change and ozone depletion. Part II: Southern Hemisphere troposphere. *J. Clim.* **2011**, *24*, 1850–1868. [[CrossRef](#)]
62. Min, S.K.; Son, S.W. Multimodel attribution of the Southern Hemisphere Hadley cell widening: Major role of ozone depletion. *J. Geophys. Res. Atmos.* **2013**, *118*, 3007–3015. [[CrossRef](#)]
63. Garfinkel, C.I.; Waugh, D.W.; Polvani, L.M. Recent Hadley cell expansion: The role of internal atmospheric variability in reconciling modeled and observed trends. *Geophys. Res. Lett.* **2015**, *42*, 10824–10831. [[CrossRef](#)]
64. Tao, L.; Hu, Y.; Liu, J. Anthropogenic forcing on the Hadley circulation in CMIP5 simulations. *Clim. Dyn.* **2016**, *46*, 3337–3350. [[CrossRef](#)]
65. Kim, B.H.; Ha, K.J. Changes in equatorial zonal circulations and precipitation in the context of the global warming and natural modes. *Clim. Dyn.* **2018**, *51*, 3999–4013. [[CrossRef](#)]
66. Henley, B.J.; Gergis, J.; Karoly, D.J.; Power, S.; Kennedy, J.; Folland, C.K. A Tripole Index for the Interdecadal Pacific Oscillation. *Clim. Dyn.* **2015**, *45*, 3077–3090. [[CrossRef](#)]
67. Xie, P.; Arkin, P.A. Global monthly precipitation estimates from satellite-observed outgoing longwave radiation. *J. Clim.* **1998**, *11*, 137–164. [[CrossRef](#)]
68. Sohn, B.J.; Yeh, S.W.; Schmetz, J.; Song, H.J. Observational evidences of Walker circulation change over the last 30 years contrasting with GCM results. *Clim. Dyn.* **2013**, *40*, 1721–1732. [[CrossRef](#)]
69. Wang, B.; Ding, Q. Changes in global monsoon precipitation over the past 56 years. *Geophys. Res. Lett.* **2006**, *33*, 1–4. [[CrossRef](#)]
70. Ha, K.J.; Moon, S.; Timmermann, A.; Kim, D. Future Changes of Summer Monsoon Characteristics and Evaporative Demand Over Asia in CMIP6 Simulations. *Geophys. Res. Lett.* **2020**, *47*, 1–10. [[CrossRef](#)]
71. Kitoh, A.; Yukimoto, S.; Noda, A.; Motoi, T. Simulated Changes in the Asian Summer Monsoon at Times of Increased Atmospheric CO₂. *J. Meteorol. Soc. Japan* **1997**, *75*, 1019–1031.
72. Conroy, J.; Overpeck, J.T.; Cole, J. El Niño/Southern Oscillation and changes in the zonal gradient of tropical Pacific sea surface temperature over the last 1.2 ka. *Pages News* **2010**, *18*, 32–34. [[CrossRef](#)]
73. Wang, B.; Luo, X.; Yang, Y.M.; Sun, W.; Cane, M.A.; Cai, W.; Yeh, S.W.; Liu, J. Historical change of El Niño properties sheds light on future changes of extreme El Niño. *Proc. Natl. Acad. Sci. USA* **2019**, *116*, 22512–22517. [[CrossRef](#)] [[PubMed](#)]

